Carbon 127 (2018) 21–30

Contents lists available at ScienceDirect

Carbon

journal homepage: www.elsevier.com/locate/carbon

Formation mechanism for oxidation synthesis of carbon nanomaterials and detonation process for core-shell structure

Boyang Liu [a, *], Shuyu Ke [a], Yingfeng Shao [b, **], Dechang Jia [c], Chunhua Fan [a], Fuhua Zhang [a], Runhua Fan [a]

[a] College of Ocean Science and Engineering, Shanghai Maritime University, Shanghai 201306, China
[b] State Key Laboratory of Nonlinear Mechanics, Institute of Mechanics, Beijing 100190, China
[c] Institute for Advanced Ceramics, Harbin Institute of Technology, Harbin 150001, China

ARTICLE INFO

Article history:
Received 2 August 2017
Received in revised form
13 October 2017
Accepted 24 October 2017
Available online 26 October 2017

ABSTRACT

A novel formation mechanism according to the oxidative dehydrogenation of organics has been proposed for the low-temperature preparation of carbon-based nanomaterials. Several typical organics including ethanol, 1-butanol, *p*-cymene and liquid paraffin are used as precursors to react with ammonium persulfate (APS) in an autoclave, and carbon particles are obtained as a validation. The reaction characteristics are comprehensively investigated by the differential scanning calorimetric and thermogravimetric analysis. The strongly exothermic oxidation reaction below 200 °C is a common feature during the process. The organic molecules are cleaved into small carbon species and further transform to amorphous carbon. When the organometallic compound is used as a reactant instead, such as magnesocene and allyltriphenyltin, carbon encapsulated MgO and SnS nanocrystals with core-shell structure are synthesized, respectively. A detonation introduced by the violent reaction occurs in the process with a very rapid liberation of heat and large quantities of thermally expanding gases. The large amounts of free atomic/radical species and reactive intermediates are generated as sources for the core-shell structure. It is a common strategy for the large scale production of carbon encapsulated oxide/sulfide nanocrystals by means of the moderate detonation process of the organometallic compound and APS in an autoclave.

© 2017 Elsevier Ltd. All rights reserved.

1. Introduction

Since the discovery of fullerene and carbon nanotube, carbon nanomaterials have attracted considerable attention because of their unique structures and properties that are clearly different from the traditional carbon phases like graphite, diamond and amorphous carbon [1,2]. A variety of novel carbon nanomaterials is successively synthesized in the last three decades, such as onion [3], nanocone [4], nanobelt [5], graphene [6] and carbyne [7]. Several universal preparation methods for the carbon nanomaterials have been developed, and the principal formation mechanisms are well understood. These methods can be illustrated in a temperature-relative oxygen content schematic (Fig. 1). And the characteristics of carbon nanomaterials synthesized by these methods can be summarized in Table 1.

First, it is necessary to define an oxidation temperature region of carbon nanomaterials (Region ①). It is commonly known that the oxidation of carbon takes place at a high temperature in the ambient atmosphere. Thus oxygen is usually eliminated in the traditional synthesis process. The oxidation temperature of carbon nanomaterials is particularly dependent upon the **order degree of microstructure**. For example, the highly purified nearly defect-free single-walled carbon nanotubes start oxidation at 600 °C according to the thermogravimetric (TG) curve [8]. On the other hand, we have prepared completely amorphous carbon nanotubes without short-range lattice fringes in the high-resolution transmission electron micrographs [9], and their oxidation temperature is only about 300 °C (Supplementary data, Fig. S1). Therefore, it is obvious that all the carbon nanomaterials with different **order** degree are sensitive to oxygen in the temperature range of 300–600 °C.

High-temperature preparation techniques are most utilized for a **highly ordered** graphitic structure. Arc discharge and laser

* Corresponding author.
** Corresponding author.
E-mail addresses: byliu@shmtu.edu.cn (B. Liu), 423782932@qq.com (S. Ke), shaoyf@lnm.imech.ac.cn (Y. Shao), dcjia@hit.edu.cn (D. Jia), chfan@shmtu.edu.cn (C. Fan), fhzhang@shmtu.edu.cn (F. Zhang), rhfan@shmtu.edu.cn (R. Fan).

https://doi.org/10.1016/j.carbon.2017.10.081
0008-6223/© 2017 Elsevier Ltd. All rights reserved.

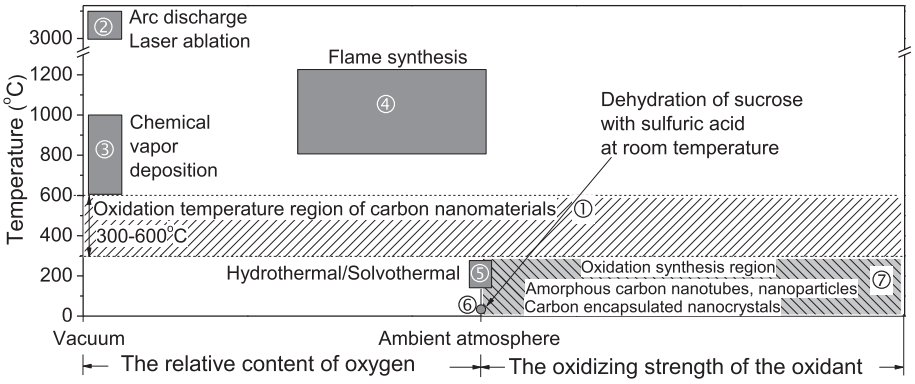

Fig. 1. The schematic illustration of synthesis methods for carbon nanomaterials.

Table 1
The characteristics of carbon nanomaterials synthesized by different methods in Fig. 1.

Method	Temperature	Typical product	Microstructure	Oxidant
Arc discharge/Laser ablation	>3000 °C	Fullerene, Nanotube, Onion	Perfectly ordered	None
CVD	600-1000 °C	Nanofiber, Nanotube, Graphene	Highly ordered	None
Flame synthesis	800-1200 °C	Nanofiber, Nanotube, Particle	Highly ordered	Deficient
Hydrothermal/Solvothermal	140-240 °C	Sphere, Nanotube	disordered	Non-essential
Oxidation synthesis	<300 °C	Particle, Nanotube, Core-shell	disordered	Essential

ablation can produce a high temperature above 3000 °C, which is sufficient for evaporation of graphite-based precursors into carbon atoms and small carbon clusters [10,11]. These gas-phase carbon sources further undergo the self-assembling process and then generate various forms of carbon nanomaterials [12–14]. Since the synthesis temperature is much higher than the oxidation temperature of carbon nanomaterials, these very energetic processes are mostly carried out in high vacuum or an inert atmosphere (Region ②). Chemical vapor deposition (CVD) is generally performed in 600–1000 °C, in which temperature range the thermal decomposition of hydrocarbons proceeds and small carbon species can be achieved for the growth of diverse carbon nanomaterials [15–17]. Both of hydrocarbons and carbon species are susceptible to oxygen at the reaction temperature. As a result, the content of oxygen in the furnace ought to be vanishingly low for the synthesis (Region ③). However, it must also be mentioned that the low concentration oxygen is not essential for the preparation of carbon nanomaterials at high temperature, flame synthesis is an alternative process using oxygen or air as the combustion medium (Region ④). The flame volume provides a carbon-rich chemically reactive environment capable of generating carbon nanostructures during a short residence time, thereby avoiding the oxidation of carbon products [18].

On the contrary, carbon nanomaterials can also be intensively fabricated in a low temperature range of 140–240 °C by the hydrothermal/solvothermal carbonization process in an autoclave (Region ⑤) [19]. Saccharides are mostly used precursors, which undergo dehydration and aromatization during the treatment and eventually give rise to carbon-rich solid products [20]. The autoclave is usually assembled in ambient atmosphere at room temperature, and the oxidation of the as-prepared carbon nanomaterials by the residual oxygen is negligible because the synthesis temperature is below the lower temperature of region ①. Otherwise, as is well-known, carbon foam will form by the dehydration reaction of sugar with concentrated sulfuric acid (a strong oxidizing agent) at room temperature (Region ⑥). According to these two processes, it is convincing that carbon can be stably obtained under 300 °C regardless of the existence of oxidizing agent.

Since the low-temperature formation of carbon is feasible, it is further assumed that with the addition of oxidizing agents carbon can form below 300 °C by an oxidation of organic compounds that are made of carbon skeletons with lots of hydrogen atoms (Region ⑦). The oxidation reaction involves the removal of hydrogen from an organic molecule and retention of carbon for nanostructures. It is plausible that the oxidizing strength of the oxidant should be one of the key factors for the formation of carbon nanomaterials. In fact, various carbon nanomaterials have been synthesized on the basis of this formation mechanism. Urones-Garrote et al. prepared carbon nanotubes and nanobags by the reaction of ferrocene with pure chlorine in a tube furnace at 200 °C [21]. At the same temperature, with the presence of ammonium chloride, we have fabricated amorphous carbon nanotubes and nanoparticles by the reaction of ferrocene with oxygen in ambient atmosphere and solvent, respectively [9,22]. It has also been proved that other stronger oxidants (such as ammonium persulfate (APS), ammonium dichromate and ammonium perchlorate) can play an identical role as oxygen, and carbon encapsulated nanocrystals with core-shell structure were prepared by a solid state reaction in an autoclave at about 200 °C [23]. Further, various carbon encapsulated metal oxide/sulfide nanocrystals were synthesized through the similar chemical route using APS and metallocene complexes at 200 °C, and a portion of carbon shell with clear turbostratic structure was visible [24–27]. Recently, we found that metal π-complexes containing different organic ligands were able to substitute for metallocene complexes in this reaction for core-shell structure [28]. These results illustrate a meaningful starting point for the low-temperature oxidation synthesis of carbon nanomaterials.

In these previous publications, carbon nanostructures derived from the cyclic organic ligands in π-bonded metallorganics, which is merely one type of the organic compounds and is therefore not comprehensive to support the assumption of oxidation synthesis. In addition, although tens of carbon encapsulated nanocrystals with core-shell structure have been prepared by the oxidation of metallocene complexes, the in-depth formation mechanism as well as the affecting factors are not fully elucidated. Consequently, in the present work, in order to adduce more evidence for the proposed

Table 2
Synthesis conditions of carbon particles and carbon encapsulated nanocrystals.

No.	Reactants				Autoclave vol. (ml)	Temp. (°C)	Time (min)	Major product
	Organics	Quantity (ml OR mmol)	APS	Quantity (mmol)				
#1	Ethanol	2 ml	$(NH_4)_2S_2O_8$	20	50	200	30	Carbon particles
#2	1-Butanol	2 ml		20				Carbon particles
#3	*p*-Cymene	2 ml		20				Carbon particles
#4	Liquid paraffin	2 ml		20				Carbon particles
#5	Magnesocene	5 mmol		10				MgO@C
#6	Allyltriphenyltin	5 mmol		10				SnS@C SnO_2 and C

assumption, more general organic reagents with different molecular structure and property are selected as precursors to react with APS, such as ethanol (CH_3CH_2OH), 1-butanol ($CH_3CH_2CH_2CH_2OH$), *p*-cymene ($(CH_3)_2CHC_6H_5CH_3$), liquid paraffin (C_nH_m, n = 11–24), π-bonded magnesocene ($(C_5H_5)_2Mg$, abbreviated as Cp_2Mg) and σ-bonded allyltriphenyltin ($CH_2CHCH_2Sn(C_6H_5)_3$). It is proved that carbon can actually form by the oxidative dehydrogenation of the organics and the strongly exothermic reaction results in a detonation process in the autoclave, which is crucial for the formation of carbon encapsulated nanocrystals with core-shell structure (denoted as 'formula of inner core'@C, such as MgO@C, SnS@C, and SnO_2@C).

2. Experimental

2.1. Materials and preparation

The analytically pure common organic reagents and the other two organometallic compounds were received from the Sinopharm Chemical Reagent Co. Ltd. and J&K Scientific Ltd., respectively. Carbon particles and carbon encapsulated nanocrystals were prepared by the oxidation of organics in an autoclave, and the synthesis conditions were presented in Table 2. Typically, the organic reagent and $(NH_4)_2S_2O_8$ were manually milled in a mortar and subsequently heated at 200 °C for 30 min. After cooling down to room temperature, the as-prepared black powder was washed with deionized water, and the final product was eventually obtained after drying overnight at 120 °C. In particular, the macroscopic morphology of as-prepared sample #5 and #6 obviously showed stratification phenomenon. Fluffy powder and soft powder agglomerates were respectively collected in the top and bottom of the autoclave for characterization.

2.2. Characterization

Phase characterization of the samples was performed by X-ray diffraction (XRD) using a PANalytical X'Pert PRO diffractometer (Cu K_α radiation, λ = 0.15418 nm). Raman spectra were measured by a Bruker Senterra micro Raman spectrometer (2 mW excitation at 633 nm). The morphology and microstructure of the samples were analyzed by scanning electron microscopy (SEM, JEOL JSM 7500F) and transmission electron microscopy (TEM, JEOL JEM 2010) equipped with an X-ray energy-dispersive spectroscopy system (EDS, EDAX) for composition analysis. Differential scanning calorimetry (DSC) and TG analysis were carried out at ambient atmosphere on a simultaneous thermal analyzer NETZSCH STA 449 F3 with a heating rate of 10 °C min^{-1} using an open alumina pan. Sealed aluminum pan was also used to simulate the reaction in the autoclave, which was conducted on NETZSCH DSC 204F1.

3. Results and discussion

In previous studies, lots of metal π-complexes with sandwich-like structure have already been used as precursors for the preparation of carbon nanomaterials. Therefore, in the first four samples, we want to verify whether other common organic reagents without metal atom in the molecule are effective as well for the oxidation synthesis of carbon. The XRD patterns of sample #1-#4 are shown in Fig. 2a. All the patterns have a very broad peak between 20 and 30°, which is a striking characteristic of amorphous structure. Otherwise, the diffraction peak of sample #2 is sharper than others, and the small shoulder around 44° corresponding to the (101) plane of graphite is visible either, suggesting the **order degree** of this sample is relatively high. It can be further proved by the Raman spectra in Fig. 2b. The two typical D and G band Raman shifts

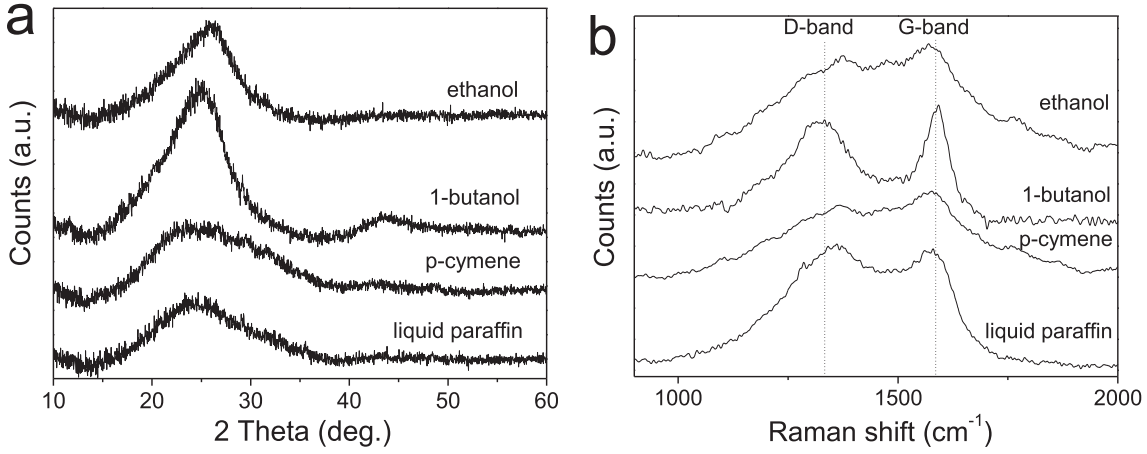

Fig. 2. XRD patterns (a) and Raman spectra (b) of the sample #1-#4.

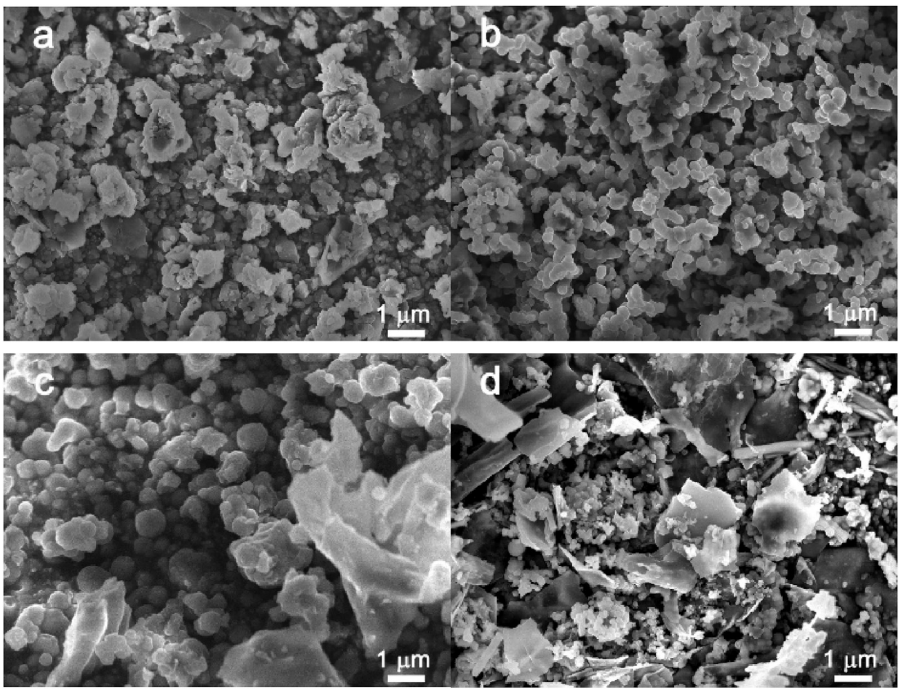

Fig. 3. SEM images of the different samples: (a) #1, (b) #2, (c) #3, (d) #4.

located at 1350 and 1580 cm^{-1} in sample #2 can be assigned to disordered carbon and **ordered** graphite, respectively [29]. The intensity ratio of the D to G band is a widely used indication of the carbon order degree [30]. The two bands of approximately equal intensity demonstrate that amorphous carbon with lattice distortion is obtained in this sample. However, the high-intensity D band and broader G band of sample #4 imply a worse **order** degree, and the two broad and overlapped bands in sample #1 and #3 belong to completely amorphous carbon [31]. Consequently, it is concluded that oxidation of organics below 300 °C is valid for the preparation of amorphous carbon and the low synthesis temperature has an adverse effect on the formation of **highly ordered** structure.

SEM images of the first four samples are displayed in Fig. 3. A large amount of micro-/nano-sized irregular-shaped particles is found in most samples except for sample #2, which is exclusively constituted of homogeneous connected nanoparticles with a diameter of 200–400 nm. The high-resolution TEM (HRTEM) images in Fig. 4 further reveal the microstructure these carbon particles. Roughly parallel short lattice fringes referred as turbostratic structure only appear in the particles of sample #2. Conversely, other samples do not have clear fringes, suggesting a completely amorphous structure. It is consistent with the XRD and Raman results that sample #2 has a relatively **high order** degree in these samples.

The reaction behaviors of the reactants in sample #1-#4 were carried out by DSC using sealed pans to closely simulate the conditions in the autoclave. Fig. 5 shows the DSC curves of these samples with an exothermic peak in common, which should be caused by the oxidation of hydrogen atom in organic reagents. The exothermic reaction of ethanol with APS starts at about 108 °C according to the onset temperature in sample #1, illustrating that ethanol can be easily oxidized to carbon. Subsequently, a sharp endothermic peak appears when the temperature increases to 119 °C, probably resulting from some side reaction. It is similar to sample #3 with the aspect of the existence of both exothermic and endothermic peaks. But the *p*-cymene is too stable to be oxidized until the temperature is raised to 168 °C. For sample #2, after a broad endothermic peak, a very sharp exothermic peak located at 168 °C can be observed, which means a violent oxidation reaction takes place and completes in a short time. Otherwise, the wide exothermic peak initiated at 179 °C in sample #4 may be attributed to the continuous oxidation of various hydrocarbons with different carbon atoms in the liquid paraffin. As a result, it is deduced that alcohols with different alkyl chains, alkanes, as well as aromatic hydrocarbons can serve as the precursors and their exothermic oxidation is vital importance for the formation of carbon. However, the accompanying endothermic side reaction will reduce the inner temperature in the autoclave, thereby weaken the oxidation reaction and lead to the generation of completely amorphous carbon, such as sample #1 and #3. And then, the dominant strongly exothermic oxidation with a large amount of heat release will rapidly increase the temperature, which is conducive to the synthesis of relatively **highly ordered** carbon (sample #2 and #4).

As mentioned above, the oxidation formation mechanism for carbon is proved to be effective. However, the morphology and microstructure of the products are the lack of novelty because only amorphous carbon particles are obtained. Therefore, it will be a meaningful investigation to develop a process for novel nanostructures based on this theory. For sample #2, the huge heat release in a short time is likely to break the 1-butanol into clusters and radicals, resulting in the formation of homogeneous carbon nanoparticles with a relatively **highly ordered structure**. In fact, large amounts of heat and gas (building up a sudden substantial pressure) generated rapidly enough constitute the detonation process, made of violent chemical transformation of an explosive. This technique is particularly in relation to nanodiamond synthesis [32], and is also widely used for the preparation of core-shell nanostructures [33–35]. During the reaction process, the detonation of carbon- and metal-containing precursors can yield a high-temperature and high-pressure state for simultaneously self-assembling of the carbon and metal clusters into core-shell structure. Hence, it is appreciable that the explosion occurred in the low-

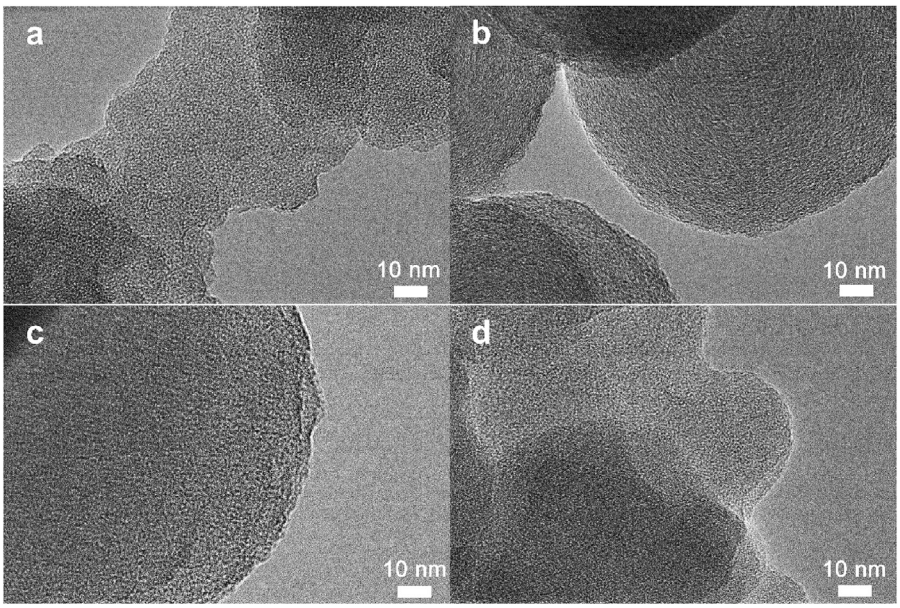

Fig. 4. HRTEM images of the different samples: (a) #1, (b) #2, (c) #3, (d) #4.

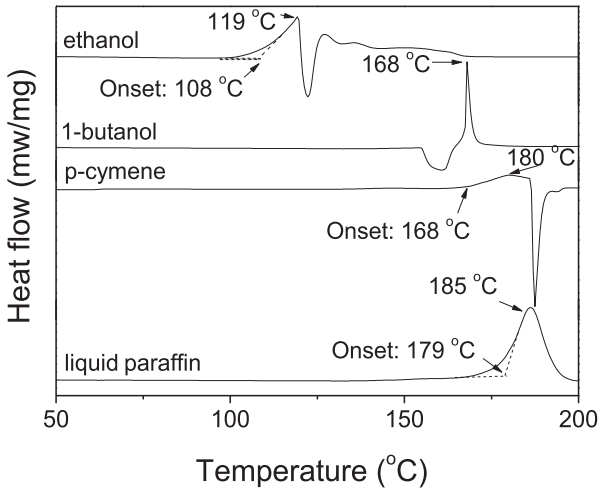

Fig. 5. DSC curves of the reactants in sample #1-#4 using sealed pans.

temperature oxidation synthesis should have the same effect for the preparation of carbon encapsulated nanocrystals with core-shell structure. The organometallic compound with metal-carbon bond ought to serve as the precursor for the carbon shell and interior nanocrystals, and both π- and σ-bonded compounds were chosen for testing the hypothesis (sample #5 and #6).

Core-shell structure has already been successfully fabricated using the precursor of metallocene complex consisting cyclopentadienyl rings bound to the transition metal, whereas magnesocene with alkaline-earth metal (magnesium) as a central metal atom is used instead in sample #5. The XRD patterns in Fig. 6a show that the sharp peaks of the top powder located at 37°, 43° and 63° can be well indexed to the cubic MgO phase with good **crystallization**. Notably, unlike the previous core-shell structures without distinct carbon diffraction peaks [23–25], the strong and wide (002) graphite peak around 26° appears in the composite, indicating that the **order degree** of the carbon shell is greatly improved. The $(NH_4)_2SO_4$ and $(NH_4)_3H(SO_4)_2$ came from the decomposition of APS are the major phases in the as-prepared bottom powder. When these soluble ammonium salts are eliminated by the washing process, the MgO and graphite diffraction peaks become visible, which is identical with the top powder. The core-shell structure can be directly observed by the SEM images of top powder, consisting of interconnected nanoparticles with obvious white cores inside (Fig. 6b and c). The homogeneous core-shell structure is the dominant product as well in the washed bottom powder (Fig. S2), which is in accordance with the XRD result. TEM and HRTEM images in Fig. 6d–f indicate the wormlike carbon shell entirely encapsulated a lot of aggregated nanocrystals, which can be indexed to the MgO (200) and (020) lattice fringes at about 0.21 nm in the enlarged image. In addition, the clear carbon fringes have a preferential curved orientation toward the center but not all the layers are well-aligned, resulting the wide (002) peak in the XRD pattern. The oxidation temperature of the MgO@C is as high as 570 °C, strongly demonstrating the good **crystallization** of the carbon shell (Fig. S3). The non-graphitizing carbon tends to crystallize in the presence of the molten alkali metals at a mild temperature (350–800 °C) [36,37]. The sodium and potassium borohydride also enable the enhancement of graphitized state by a solvothermal method at 320–350 °C, respectively [31]. However, the transformation mechanism made by the alkali metal and its compound is still not well interpreted. It is believed that the magnesium atom in the precursor have the same effect as sodium because of their similar valence properties, which needs further investigation.

Allyltriphenyltin is the first σ-bonded complex used for the preparation of core-shell structure (sample #6). Black fluffy powder is collected in the top of the autoclave and its XRD pattern is shown in Fig. 7aI. The orthorhombic phase of SnS is the major product while carbon diffraction peak is absent. Besides the black agglomerates, some white powder can also be found in the bottom of the autoclave. The XRD pattern shows that the mixture is abundant of $(NH_4)_3H(SO_4)_2$ with good **crystallization** (Fig. 7aII). After washing, only black powder is remained, which is composed of a majority of SnO_2 and a small amount of SnS (Fig. 7aIII). All the SnO_2 peaks are very broad because of its small size. Under SEM examination, the homogeneous nanoparticles in the top powder exhibit an equiaxed

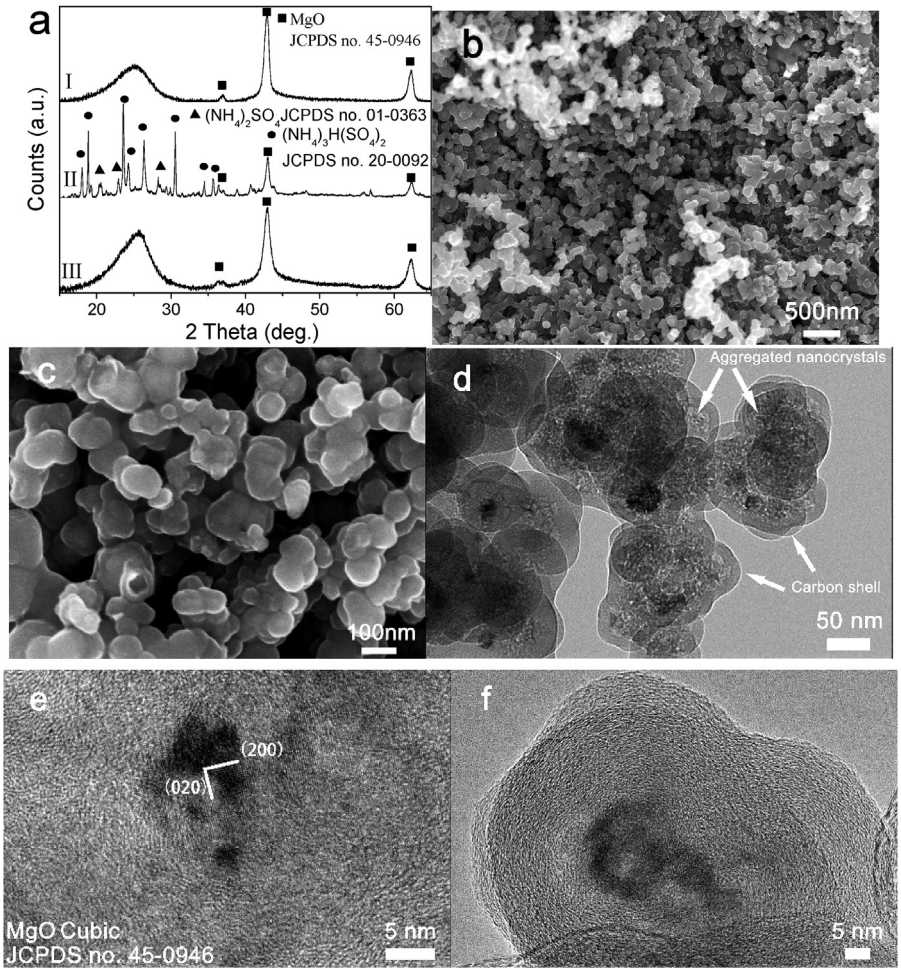

Fig. 6. (a) XRD patterns of the powder in sample #5 in the different position of the autoclave: (I) top, (II) bottom, (III) washed bottom. (b, c) SEM images of the top powder at different magnifications. (d–f) TEM and HRTEM images of the top powder.

morphology and aggregate together (Fig. 7b). The semitransparent carbon layer and the white inner cores corresponding to the core-shell structure are further revealed in the high magnification image (Fig. 7c). The uniformity of the washed bottom power is slightly decreased due to the emergence of some large particles, as indicated by the arrows (Fig. 7d). In the enlarged image (Fig. 7e), the core-shell structure and a lot of agglomerates (indicated by white arrows) consisted of ultrafine nanocrystals appear simultaneously. From the TEM image in Fig. 7f, the large spherical particles with a diameter of 200–400 nm and small aggregated nanocrystals are both encapsulated by the carbon shell in the top powder. The EDS spectrum of the large particles demonstrates that C, S and Sn are the major elements with the S/Sn molar ratio close to the SnS stoichiometry (Fig. S4). In the HRTEM image of Fig. 7g, the small nanocrystal can be perfectly indexed to the SnS phase and the carbon shell is amorphous because of its disordered fringes. The DSC-TG curves also show that the carbon shell is more vulnerable to oxygen than that of sample #5 owing to its low initial oxidation temperature of 445 °C, as shown in Fig. S5. The agglomerates in the bottom powder can also be indicated by the white arrows (Fig. 7h), which are actually composed of ultrafine SnO_2 nanocrystals with a diameter of about 5 nm (Fig. 7i). The carbon shell on these nanocrystals is not discernible, which may lead to the existence of white colored as-prepared powder in the bottom. However, the carbon characteristic peak in the EDS spectrum illustrates that a small amount of carbon is probably distributed in the gap between the nanocrystals (Fig. S6), and the agglomerates can be conceived as SnO_2/Carbon composite. Otherwise, a small quantity of SnO_2@C with core-shell structure can also be observed in the bottom powder, as shown in Fig. S7. Therefore, the core-shell structure is the dominant product in sample #6.

Thermal analysis using different pans is essential to investigate the reaction behavior of the reactants in sample #5 and #6, as shown in Fig. 8. In an open pan, the measurement is conducted in the air atmosphere, and the weight change during the reaction can be recorded by the TG curve. On the other hand, the sealed pan is likened to the autoclave, and the reaction characteristic is revealed in the DSC curve. The pure APS is definitely stable in the open pan until the temperature is increased to 185 °C (Fig. 8a), and it will decompose into ammonium pyrosulfate and oxygen [38]. In sample #5, the sublimation of Cp_2Mg results in the sluggish weight loss from 100 °C, and the reaction actually takes place at 178 °C indicated by the 3% sharp weight loss in the TG curve. Since the time resolution of the TG measurement is 100 ms (10 data points per second) [39], the typical reaction time is about 100 ms or less (Table S1). Taking into account the small sublimation weight loss before the reaction, the reaction enthalpy is qualitatively calculated to be 347 J/g by integrating the area under the strongly endothermic peak (Fig. S8). For pure APS in the sealed pan (Fig. 8b), another small exothermic peak appeared at 132 °C should be caused by some side reaction of APS, and the reaction products may further accelerate the decomposition of APS because the

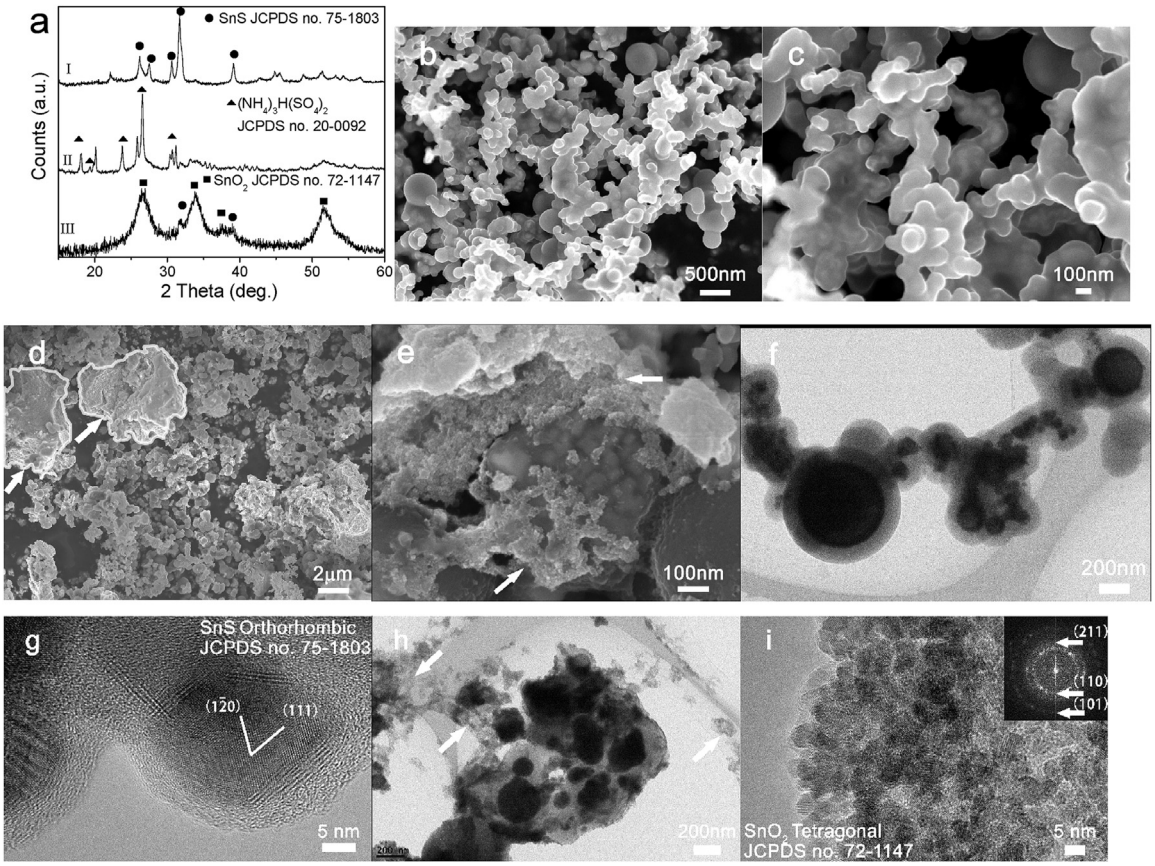

Fig. 7. (a) XRD patterns of the powder in sample #6 in the different position of the autoclave: (I) top, (II) bottom, (III) washed bottom. SEM images of (b, c) the top powder and (d, e) the washed bottom powder at different magnifications. TEM and HRTEM images of the (f, g) top powder and (h, i) the washed bottom powder. Inset in (i) is the corresponding fast Fourier transform (FFT) pattern.

corresponding peak is advanced to 170 °C. However, the former peak is absent in the mixture of Cp_2Mg and APS, which can be explained that APS has already participated in some side reaction without heat absorption/release. The two strong and overlapped exothermic peaks started at 148 °C is an evidence for the severe oxidation reaction. For sample #6, the DSC-TG curves are similar to that of sample #5, while the difference is an endothermic transition coincided with the melt of allyltriphenyltin can be found at about 75 °C. In the open pan (Fig. 8c), some melted allyltriphenyltin will be blown off by the purge gas above 125 °C, and the oxidation reaction initiates at 193 °C with a 14% linear decrease in the TG curve. This reaction is ultrafast and has completed within 200 ms (Table S2), moreover the accompanying exothermic reaction has an enthalpy of 292 J/g (Fig. S9). It is noticeable that although the reaction temperature of the mixture is higher than the decomposition temperature of pure APS, the typical exothermic peak and weight loss belong to the decomposition of pure APS cannot be found, proving some side reaction has taken place at a lower temperature. In the seal pan, the reaction of allyltriphenyltin with APS is also quite violent determined by the strong and narrow exothermic peak at 195 °C (Fig. 8d). Consequently, from the above results, the extremely fast exothermic energy release with concurrent weight loss is the obvious feature during the oxidation of the organometallic compound, which is the same as some metallocene complexes [24,26,40].

On further discussion, there are three features like most explosive chemical reactions evolving heat and pressure and can be regarded as important factors for the formation of core-shell structure. First, the generation of heat in large quantities accompanies the oxidation of organometallic compound. Most of the organometallic compounds as well as the organics will be oxidized by APS in the temperature range of 100–200 °C. However, the organic ligand bonded to metal atom will enhance its chemical activity. For instance, both with benzene ring included, the oxidation temperature of *p*-cymene is lower than allyltriphenyltin. Otherwise, the σ-bonded allyltriphenyltin seems more stable concerning the π-bonded Cp_2Mg. Therefore, with the increase of temperature, the organometallic compound will be gradually oxidized, and its structure becomes unstable, though no thermal effect is observed during this period. When the oxidation temperature is reached, a violent reaction of organic ligands takes place, in which hydrogen is transformed to water with heat release. It is just the second feature that the gaseous products are produced in the reaction accounting for the rapid decline in weight. Third, the kinetics of decomposition is ultrafast and proceeds typically in 100 ms or less traced by TG measurement. These features can be vividly visualized by heating the mixture of allyltriphenyltin and APS in an open bottle, which is simultaneously recorded by both general and infrared camera (Video S1). Like a volcanic eruption, large amounts of heat and gas are instantaneously formed in the sudden reaction, rapidly raising the temperature in the bottle. The liberation of heat with sufficient rapidity is a necessary factor that is responsible for an explosion. However, the brown-colored powder collected in the open bottle signifies inadequate carbonization of the precursor, which is completely different with that in the autoclave (Fig. S10). It has exemplified by the reaction of ferrocene with APS that the sealed reactor is vital to the formation of core-shell structure [24].

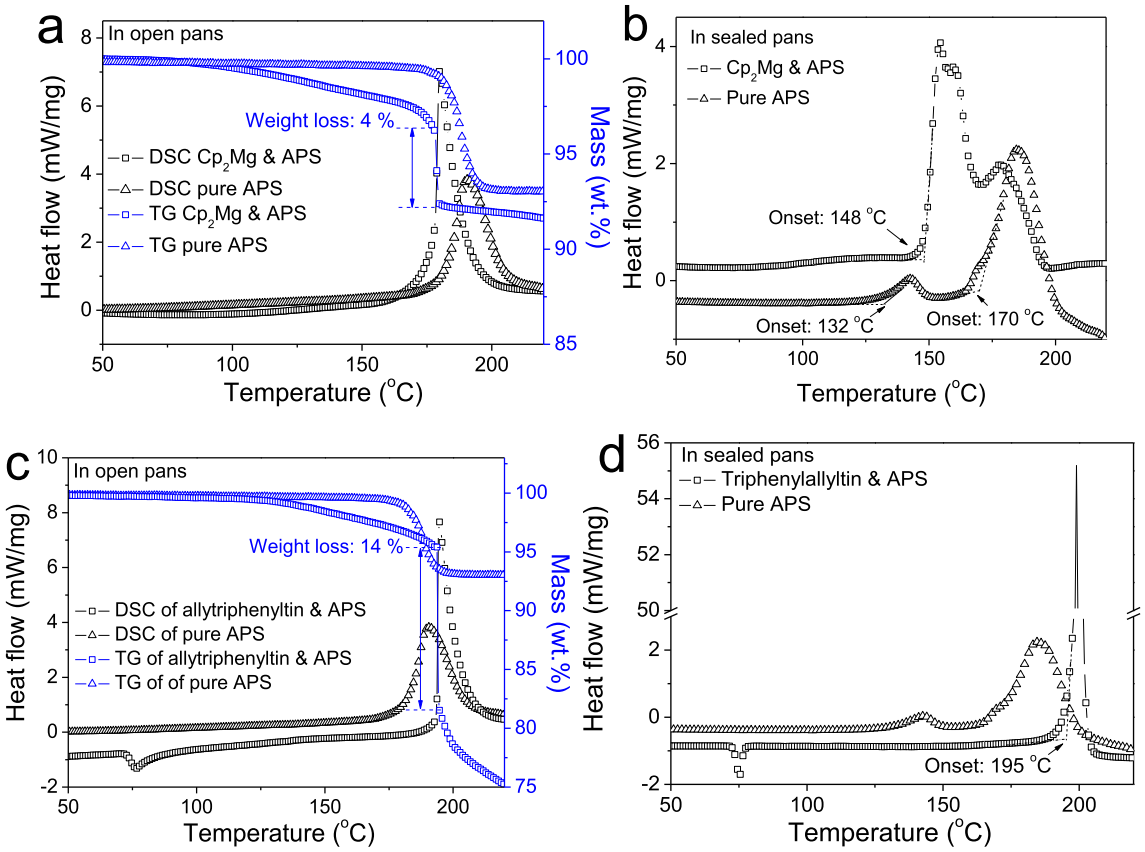

Fig. 8. DSC-TG and DSC of the reactants in different pans: (a, b) sample #5, (c, d) sample #6. (A colour version of this figure can be viewed online.)

Supplementary video related to this article can be found at https://doi.org/10.1016/j.carbon.2017.10.081.

When the reaction is transferred into an autoclave, the very rapid liberation of heat and large quantities of thermally expanding gases are confined in the space and cannot be dissipated to the external environment. The exertion of extremely high pressure on the surrounding medium forms a propagating shock wave with a high velocity, which can be perceived as a detonation process. The schematic of the detonation process and the formation mechanism for core-shell structure are proposed in Fig. 9. The violent reaction quickly accelerates through the reacted part of the sample toward the unreacted site. The shock-wave front with a high temperature and pressure gradient instantaneously initiates an intensive chemical transformation of the sample in an exceedingly thin layer adjacent to the wave front (chemical reaction zone) [41]. The exothermic chemical energy liberated in the chemical reaction zone by the non-equilibrium chemical processes continuously maintains a high pressure in the shock wave and self-sustains the detonation process [42]. In this zone, the organometallic compound and APS molecules are torn apart and broken down into free

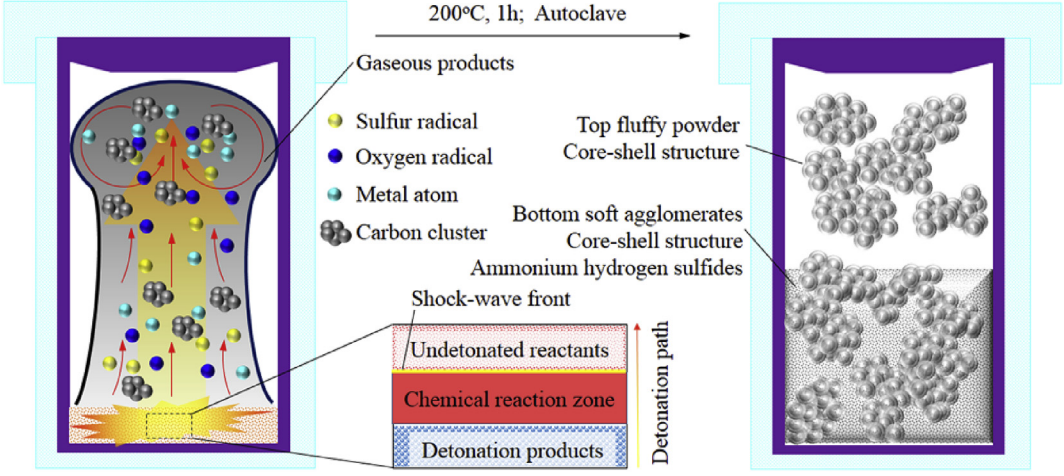

Fig. 9. The schematic of the detonation process and the formation mechanism for core-shell structure. (A colour version of this figure can be viewed online.)

atomic/radical species and reactive intermediates, including sulfur and oxygen radicals, metal atom, carbon clusters, and different kinds of gas atmospheres, which are sources for the generation of core-shell structure [43]. Then, nucleation occurs and growth stage takes place in a very short time at a high pressure. Nevertheless, the relatively low temperature is generally not beneficial to grow large crystals and form a long-range ordered carbon. In addition, the abundant carbon clusters also serve as a barrier to inhibit the aggregation of the nanocrystals. Therefore, amorphous carbon shell encapsulated fine metal oxide/sulfide nanocrystals are commonly obtained. The gaseous products flow in the same direction as that of the propagation of detonation. Some of the atomic/radical species and reactive intermediates can be blown to the upper zone of the autoclave by the steam, and the ammonium hydrogen sulfate salts from the decomposition of APS are stayed at the bottom, leading to the macroscopic morphology difference of the last two sample. In sample #6, aside from the SnS@C, the SnO_2 nanocrystals without carbon shell may be formed owing to the stable benzene ligands, which are not susceptible to oxidation and the complete cleavage of C—C bond into small carbon radicals is relatively difficult. It is also suggested that a fast heating rate can decrease the side reaction before the detonation, thereby reduce the irregular shaped byproducts.

Actually, APS is a stable and safe oxidizing agent, not capable of explosion on its own. But the mixture of organometallic compound and APS is a stable explosive, and its detonation is excited by the input of heat energy. Then, it supplies its own oxygen for detonation and continues by itself until completion, which does not rely on the atmosphere. The decomposition enthalpy in sample #5 and #6 is only about several hundred Joule per gram, which is much lower than that of gunpowder (2800 J/g) [44]. Therefore, the mixture should be classified as a novel low explosive as compared with the gunpowder and other high explosives such as TNT and RDX. The brisance of the detonation can be easily dissipated, and the process is highly controllable and safe.

To sum up, carbon encapsulated nanocrystals with core-shell structure can be commonly synthesized by a moderate detonation process of organometallic compound and APS in an autoclave. Thousands of organometallic compounds containing various metal, metalloid and nonmetal elements bonded to organic ligands can be used as precursors. A variety of oxides and sulfides can be fabricated as inner cores. On the other hand, the detonation temperature is less than 200 °C, and there is also no need to worry about the oxidation of the carbon shell. So no special instrument is required for the synthesis except a sealed reactor to resist the internal pressure. Moreover, the process is very efficient, simple and suitable for large scale production, which has practical utility in industry and commerce.

4. Conclusions

Several carbon-based nanomaterials are successfully prepared via the reaction of organic precursors with APS in the autoclave. The strongly exothermic reaction below 200 °C is a common feature in these synthesis, corresponding to the oxidative dehydrogenation of the precursors, which are cleaved into small carbon species and further transform to amorphous carbon. It is validated that the low-temperature oxidation of organics is effective for the synthesis of carbon nanomaterials. Carbon encapsulated nanocrystals with core-shell structure can also be commonly formed under a mild detonation condition of organometallic compound and APS. The rapid release of a large amount of heat and gas is crucial for the formation of core-shell structure. The method is suitable for large scale of production of various carbon encapsulated metal oxide/sulfide nanocrystals for the potential applications in batteries and environmental cleaning in terms of the simple process, low energy consumption and high efficiency.

Acknowledgements

This work is sponsored by Natural Science Foundation of Shanghai (14ZR1419400, 15ZR1420500), National Natural Science Foundation of China (11572326), Strategic Priority Research Program of the Chinese Academy of Sciences (XDB22040102) and Opening fund of State Key Laboratory of Nonlinear Mechanics.

Appendix A. Supplementary data

Supplementary data related to this article can be found at https://doi.org/10.1016/j.carbon.2017.10.081.

References

[1] M.S. Dresselhaus, G. Dresselhaus, P.C. Eklund, Science of Fullerenes and Carbon Nanotubes: Their Properties and Applications, Academic Press, 1996.
[2] R. Saito, G. Dresselhaus, M.S. Dresselhaus, Physical Properties of Carbon Nanotubes, World scientific, 1998.
[3] N. Sano, H. Wang, M. Chhowalla, I. Alexandrou, G. Amaratunga, Nanotechnology: synthesis of carbon'onions' in water, Nature 414 (6863) (2001) 506–507.
[4] Z. Tsakadze, I. Levchenko, K. Ostrikov, S. Xu, Plasma-assisted self-organized growth of uniform carbon nanocone arrays, Carbon 45 (10) (2007) 2022–2030.
[5] C.T. Lin, T.H. Chen, T.S. Chin, C.Y. Lee, H.T. Chiu, Quasi two-dimensional carbon nanobelts synthesized using a template method, Carbon 46 (5) (2008) 741–746.
[6] M. Losurdo, M.M. Giangregorio, P. Capezzuto, G. Bruno, Graphene CVD growth on copper and nickel: role of hydrogen in kinetics and structure, Phys. Chem. Chem. Phys. 13 (46) (2011) 20836–20843.
[7] L. Shi, P. Rohringer, K. Suenaga, Y. Niimi, J. Kotakoski, J.C. Meyer, H. Peterlik, M. Wanko, S. Cahangirov, A. Rubio, Z.J. Lapin, L. Novotny, P. Ayala, T. Pichler, Confined linear carbon chains as a route to bulk carbyne, Nat. Mater. 15 (6) (2016) 634–639.
[8] Y. Liu, L. Gao, J. Sun, S. Zheng, L. Jiang, Y. Wang, H. Kajiura, Y. Li, K. Noda, A multi-step strategy for cutting and purification of single-walled carbon nanotubes, Carbon 45 (10) (2007) 1972–1978.
[9] B. Liu, D. Jia, Y. Zhou, H. Feng, Q. Meng, Low temperature synthesis of amorphous carbon nanotubes in air, Carbon 45 (8) (2007) 1710–1713.
[10] J. Hutchison, N. Kiselev, E. Krinichnaya, A. Krestinin, R. Loutfy, A. Morawsky, V. Muradyan, E. Obraztsova, J. Sloan, S. Terekhov, Double-walled carbon nanotubes fabricated by a hydrogen arc discharge method, Carbon 39 (5) (2001) 761–770.
[11] C.D. Scott, S. Arepalli, P. Nikolaev, R.E. Smalley, Growth mechanisms for single-wall carbon nanotubes in a laser-ablation process, Appl. Phys. A 72 (5) (2001) 573–580.
[12] Z. Shi, Y. Lian, X. Zhou, Z. Gu, Y. Zhang, S. Iijima, L. Zhou, K.T. Yue, S. Zhang, Mass-production of single-wall carbon nanotubes by arc discharge method, Carbon 37 (9) (1999) 1449–1453.
[13] N. Li, Z. Wang, K. Zhao, Z. Shi, Z. Gu, S. Xu, Large scale synthesis of N-doped multi-layered graphene sheets by simple arc-discharge method, Carbon 48 (1) (2010) 255–259.
[14] S. Iijima, M. Yudasaka, R. Yamada, S. Bandow, K. Suenaga, F. Kokai, K. Takahashi, Nano-aggregates of single-walled graphitic carbon nano-horns, Chem. Phys. Lett. 309 (3) (1999) 165–170.
[15] W. Wang, Y. Lin, C. Kuo, Nanofabrication and properties of the highly oriented carbon nanocones, Diam. Relat. Mater. 14 (3) (2005) 907–912.
[16] A.M. Cassell, J.A. Raymakers, J. Kong, H. Dai, Large scale CVD synthesis of single-walled carbon nanotubes, J. Phys. Chem. B 103 (31) (1999) 6484–6492.
[17] S.C. O'Hern, C.A. Stewart, M.S. Boutilier, J.-C. Idrobo, S. Bhaviripudi, S.K. Das, J. Kong, T. Laoui, M. Atieh, R. Karnik, Selective molecular transport through intrinsic defects in a single layer of CVD graphene, ACS Nano 6 (11) (2012) 10130–10138.
[18] W. Merchan-Merchan, A.V. Saveliev, L. Kennedy, W.C. Jimenez, Combustion synthesis of carbon nanotubes and related nanostructures, Prog. Energy Combust. 36 (6) (2010) 696–727.
[19] B. Hu, K. Wang, L. Wu, S.H. Yu, M. Antonietti, M.M. Titirici, Engineering carbon materials from the hydrothermal carbonization process of biomass, Adv. Mater. 22 (7) (2010) 813–828.
[20] M. Sevilla, A.B. Fuertes, The production of carbon materials by hydrothermal carbonization of cellulose, Carbon 47 (9) (2009) 2281–2289.
[21] E. Urones-Garrote, D. Ávila-Brande, N. Ayape-Katcho, A. Gómez-Herrero, A.R. Landa-Cánovas, L.C. Otero-Díaz, Amorphous carbon nanostructures from chlorination of ferrocene, Carbon 43 (5) (2005) 978–985.
[22] B. Liu, H. Huang, F. Zhang, Y. Zhou, W. Li, J. Zhang, Agglomerates of amorphous

carbon nanoparticles synthesized by a solution-phase method, Mater. Lett. 66 (1) (2012) 199–202.
[23] B. Liu, N. Zhong, C. Fan, Y. Zhou, Y. Fan, S. Yu, F. Zhang, L. Dong, Y. Yin, Low temperature synthesis and formation mechanism of carbon encapsulated nanocrystals by electrophilic oxidation of ferrocene, Carbon 68 (2014) 573–582.
[24] B. Liu, C. Fan, J. Chen, J. Wang, Z. Lu, J. Ren, S. Yu, L. Dong, W. Li, Low temperature in situ synthesis and the formation mechanism of various carbon-encapsulated nanocrystals by the electrophilic oxidation of metallocene complexes, Nanotechnology 27 (7) (2016) 075603.
[25] B. Liu, C. Fan, J. Chen, Y. Zhou, L. Dong, J. Wang, Low temperature one-step synthesis of carbon co-encapsulated NiS 2, NiS and S 8 nanocrystals by electrophilic oxidation of nickelocene, Mater. Lett. 142 (2015) 90–93.
[26] B. Liu, Y. Shao, Y. Zhang, F. Zhang, N. Zhong, W. Li, Highly efficient solid-state synthesis of carbon-encapsulated ultrafine MoO2 nanocrystals as high rate lithium-ion battery anode, J. Nanopart. Res. 18 (12) (2016) 375.
[27] B. Liu, F. Zhang, Q. Wu, J. Wang, W. Li, L. Dong, Y. Yin, Low temperature synthesis of carbon encapsulated Fe 7 S 8 nanocrystals as high performance anode for lithium-ion batteries, Mater. Chem. Phys. 151 (2015) 60–65.
[28] B. Liu, Y. Shao, X. Xiang, F. Zhang, S. Yan, W. Li, Highly efficient one-step synthesis of carbon encapsulated nanocrystals by the oxidation of metal π -complexes, Nanotechnology 28 (32) (2017) 325603.
[29] M. Pimenta, G. Dresselhaus, M.S. Dresselhaus, L. Cancado, A. Jorio, R. Saito, Studying disorder in graphite-based systems by Raman spectroscopy, Phys. Chem. Chem. Phys. 9 (11) (2007) 1276–1290.
[30] X. Xiang, L. Zhang, H.I. Hima, F. Li, D.G. Evans, Co-based catalysts from Co/Fe/Al layered double hydroxides for preparation of carbon nanotubes, Appl. Clay Sci. 42 (3) (2009) 405–409.
[31] Y. Xiong, Y. Xie, X. Li, Z. Li, Production of novel amorphous carbon nanostructures from ferrocene in low-temperature solution, Carbon 42 (8) (2004) 1447–1453.
[32] V.N. Mochalin, O. Shenderova, D. Ho, Y. Gogotsi, The properties and applications of nanodiamonds, Nat. Nanotechnol. 7 (1) (2012) 11–23.
[33] C. Cao, Z. Ma, C. Ma, W. Pan, Q. Liu, J. Wang, Synthesis and characterization of Fe/C core–shell nanoparticles, Mater. Lett. 88 (2012) 61–64.
[34] N. Luo, X. Li, X. Wang, H. Yan, C. Zhang, H. Wang, Synthesis and characterization of carbon-encapsulated iron/iron carbide nanoparticles by a detonation method, Carbon 48 (13) (2010) 3858–3863.
[35] G. Sun, X. Li, Y. Zhang, X. Wang, D.a. Jiang, F. Mo, A simple detonation technique to synthesize carbon-coated cobalt, J. Alloy Compd. 473 (1) (2009) 212–214.
[36] K.W. McNamara, P. Ayyappan, R. Rajagopalan, J.G. Chen, H.C. Foley, Localized crystallization of polyfurfuryl alcohol derived carbon by alkali metals, Carbon 56 (2013) 109–120.
[37] Z. Xu, B. Xia, W. Wang, T. Ji, C. Ma, L. Gan, Graphitization of aerogel-like carbons in molten sodium metal, Carbon 49 (10) (2011) 3385–3387.
[38] L. Erdey, S. Gal, G. Liptay, Thermoanalytical properties of analytical-grade reagents: ammonium salts, Talanta 11 (6) (1964) 913–940.
[39] S. Ichilmann, K. Rücker, M. Haase, D. Enke, M. Steinhart, L. Xue, Adiabatic burst evaporation from bicontinuous nanoporous membranes, Nanoscale 7 (20) (2015) 9185–9193.
[40] B. Liu, Y. Shao, X. Xiang, J. Ren, W. Li, Low-temperature one-step solid-phase synthesis of carbon-encapsulated TiO2 nanocrystals as anode materials for lithium-ion batteries, Ionics 23 (8) (2017) 2013–2024.
[41] S. Venugopalan, Demystifying Explosives: Concepts in High Energy Materials, Elsevier, 2015.
[42] C.M. Tarver, Detonation reaction zones in condensed explosives, in: AIP Conference Proceedings, AIP, 2006, pp. 1026–1029.
[43] Z. Liang, S. Browne, R. Deiterding, J. Shepherd, Detonation front structure and the competition for radicals, Proc. Combust. Inst. 31 (2) (2007) 2445–2453.
[44] M. Brown, R. Rugunanan, A temperature-profile Study of the combustion of black powder and its constituent binary mixtures, Propell. Explos. Pyrot. 14 (2) (1989) 69–75.